Extraordinary nonlinear transmission modulation in a doubly resonant acousto-optical structure

Vincent Laude,[1,2,*] Abderrahmane Belkhir,[1,3] Abdullah F. Alabiad,[1] Mahmoud Addouche,[1,2] Sarah Benchabane,[1,2] Abdelkrim Khelif,[1,2] and Fadi I. Baida[1,2]

[1]Institut FEMTO-ST, Université de Bourgogne Franche-Comté, 25030 Besançon, France
[2]Institut FEMTO-ST, Centre National de la Recherche Scientifique, 25030 Besançon, France
[3]Laboratoire de Physique et Chimie Quantique, Université Mouloud Mammeri, Tizi-Ouzou, Algeria
*Corresponding author: vincent.laude@femto-st.fr

Acousto-optical modulators usually rely on coherent diffraction of light by a moving acoustic wave, leading to bulky devices with a long interaction length. We propose a subwavelength acousto-optical structure that instead relies on a double resonance to achieve strong modulation at near-infrared wavelengths. A periodic array of metal ridges on a piezoelectric substrate defines cavities that create a resonant dip in the optical transmission spectrum. The ridges simultaneously support large flexural vibrations when resonantly excited by a radio-frequency signal, effectively deforming the cavities and leading to strongly nonlinear acousto-optical modulation. The nano-optical structure could find applications in highly compact photonic devices. © 2017 Optical Society of America

1. INTRODUCTION

Léon Brillouin predicted in 1922 that optical waves could be diffracted by tiny vibrations inside matter, oscillating at acoustic frequencies, whether they be generated by thermal fluctuations or coherent acoustic waves [1]. Since the first experimental demonstrations by Debye and Sears [2], and Lucas and Bicquard [3], acousto-optical (AO) interactions have been the subject of many studies and have led to various AO modulators and devices. The standard physical model of AO interaction inside materials is based on the photoelastic effect, according to which strain-stress acoustic waves form moving diffraction gratings that scatter light to preferred directions and modulate it in time at the acoustic frequency, causing a Doppler shift of the diffracted light frequency. The photoelastic effect is described as a small perturbation of the bulk optical permittivity, and it hence requires the coherent interference of waves diffracted on many-wavelength-long gratings to lead to significant AO modulation [4].

Recently, the emergence of optomechanics has attracted much attention toward another mechanism for the interaction of light and sound: the modulation of an optical resonance frequency caused by mechanical vibrations deforming a resonator. Radiation pressure exerted by light for instance causes it to couple to the deformations of a cavity, leading to unprecedentedly sensitive mass-sensing devices or light-assisted cooling down to the fundamental quantum state of the resonator [5–7]. The moving interface effect is intrinsically related to radiation pressure [8,9], and both can indeed be derived from the same Lagrangian [10] or Hamiltonian [11] formulation.

This effect is responsible for the surface AO modulation that complements the bulk photoelastic effect in nanophotonic structures [12]. It has generally been modeled as a first-order perturbation of the optical permittivity [13], following the canonical model of photoelasticity, but this assumption can be expected to break down if large deformations occur. Multiphonon AO modulation has furthermore been predicted in multilayers of simultaneous photonic and phononic crystals enclosing a defect cavity [14], and though the resulting all-solid structure could not sustain large deformations, AO nonlinearities resulted from the cavity being able to tightly confine sound and light. The problem we consider is then the following: can we design a resonant AO structure for which surface deformations at an acoustic frequency can be large enough for strong and nonlinear modulation to result from the moving interface effect?

In order to achieve the above goal, we consider the nano-optical structure depicted in Fig. 1. A subwavelength-thick optical resonator is formed by a periodic array of metal ridges that define optical cavities. One period of the array includes two asymmetric cavities that sustain an optical Fano resonance [15] that can be excited under normal incidence, causing a sharp dip in the transmission spectrum. By applying a time-harmonic external acoustic signal with the frequency tuned to a mechanical resonance of the array of ridges, flexural oscillations with large amplitude can be induced, and an extraordinary AO modulation of the transmitted light is obtained. The nonlinear regime is reached with only a few nanometers of vibration amplitude at gigahertz (GHz) frequencies.

2. OPTICAL RESONANCE

The one-dimensional array of slits defined by silver ridges shown in Fig. 1 is periodic along the x_1 direction, with lattice constant p. It is deposited on an optically transparent piezoelectric substrate, such as lithium niobate, and it is illuminated under normal incidence with near-infrared light with transverse magnetic (TM)-polarized illumination (the magnetic field is directed along the x_2 axis). One period of the structure contains two slits with the same height h but different widths w_1 and w_2. The imbalance between the slit widths is measured by the parameter $e = w_1 - w_2$. The orientation of lithium niobate is such that the Y (Z, respectively) crystallographic axis is aligned along the x_3 (x_1, resp.) reference axis. With this choice, the index of refraction of lithium niobate for TM light can be considered isotropic. We take $n = 2.2472$ constant in the range of interest, i.e., we neglect the dispersion of lithium niobate. Silver is selected for its rather small optical absorption loss. Numerical simulations were performed with a homemade finite-difference time-domain (FDTD) code including a critical points model to faithfully describe the dispersion of the dielectric constant of silver $\varepsilon(\omega)$ [16]. FDTD results were compared to a time-harmonic finite element model (FEM) to check consistency and accuracy; they were found to agree to within a relative error smaller than 1% in all considered cases. Details of the FDTD and FEM computation models may be found in Supplement 1.

Asymmetry in the unit cell, as compared to the regular symmetric grating, is known to induce a Fano—or phase—resonance [17], the optical signature of which is a narrow dip in the transmission spectrum. According to the value of e, the dip properties can be highly sensitive to local environmental changes imposed by external excitations, such as a mechanical deformation. A parametric study was performed to optimize the design so as to obtain the highest quality factor, taking into account fabrication accuracy, as detailed in Supplement 1. The determined parameters are $p = 640$ nm, $h = 270$ nm, $w = 100$ nm, and $e = 80$ nm. The optical transmission and reflection spectra are shown in Fig. 2(a). The transmission spectrum shows a dip at resonance that reaches 50% with a Q factor equal to 730. The depth of
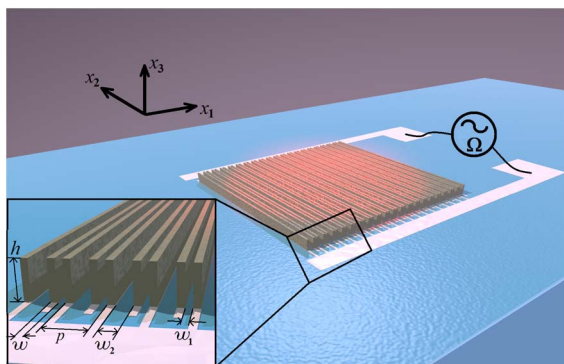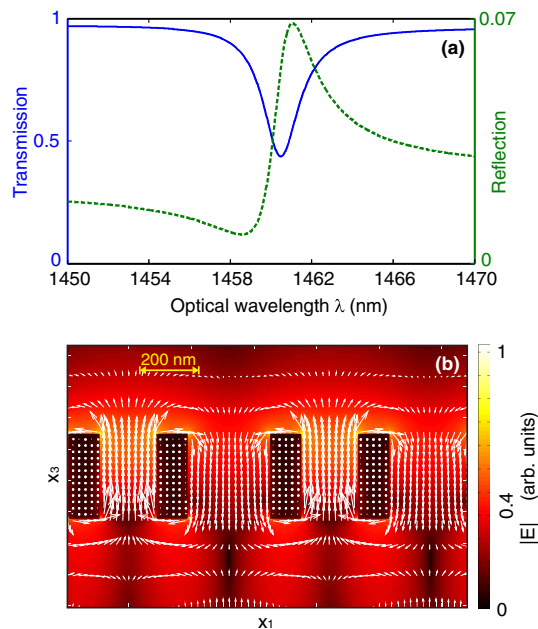

Fig. 2. Optical transmission around the Fano resonance. The structure of silver ridges on a lithium niobate substrate has parameters $h = 270$ nm, $w = 100$ nm, $p = 640$ nm, and $e = 80$ nm, with reference to Fig. 1. A normally incident TM plane wave travels upward. Transmission (T) and reflection (R) are shown in (a) as a function of optical wavelength in the region of the Fano resonance. The electric field intensity (color map) and the Poynting vector (arrows) are shown in (b) at the resonance wavelength ($\lambda = 1460.5$ nm), i.e., for the minimum transmission.

the dip is due to the substantial lifetime of photons (proportional to Q) inside the structure, which leads to enhanced light–metal interaction and, by way of consequence, to enhanced losses. Furthermore, the asymmetry of the reflection spectrum confirms the Fano character of the resonance. Figure 2(b) illustrates the electric field intensity distribution and the direction and magnitude of the Poynting vector at resonance. A strong confinement of the electric field intensity occurs at the top corners of the cavity. At resonance, the electromagnetic power flows up in the smaller slit but streams down inside the larger slit. This type of resonance was called π resonance [15] due to the fact that the electric fields within the two slits have opposite signs. The electromagnetic power loop leads to an increased photon lifetime that enhances the interaction with external excitations.

Fig. 1. Doubly resonant AO structure. w_1 and w_2 are cavity widths, w is the metal width, $p = 2w + w_1 + w_2$ is the period of the grating, and h is the metal thickness. The imbalance parameter $e = w_1 - w_2$ measures the departure from equal cavity widths. The piezoelectric substrate supporting the structure is semi-infinite. Metal ridges are alternatively connected to a current source, thus forming an elastic wave transducer. A time-harmonic electric potential difference $V(\Omega)$ is applied to drive mechanical motion at an acoustic frequency Ω.

3. ELASTIC RESONANCES

The array of silver ridges can also be used as a transducer for mechanical resonances of the ridges [18]. Electrical transduction is achieved, thanks to the piezoelectricity of the substrate, by connecting the ridges alternatively to a pair of electrical buses and applying a time-harmonic potential difference. The stress distribution created in the substrate by the spatially periodic electric field distribution excites surface acoustic waves (SAW) that, in turn, cause the ridges to vibrate. If the excitation frequency is tuned to a mechanical resonance, then rather large vibration amplitude can be expected. As a note, the velocity of the Rayleigh surface wave for the considered orientation of lithium niobate is 3487 m/s. It should be kept in mind, however, that the Rayleigh

wave is a mode of the planar free surface. For thick ridges on the surface, as considered here, there exists instead a family of surface guided waves with velocities generally slower than the Rayleigh SAW on the homogeneous surface [18]. These surface guided waves result from hybridization of the mechanical resonances of the ridges with the elastic waves propagating in the substrate.

One period of the transducer is composed of two successive ridges. Assuming that an electric potential difference V is applied using a current source at angular frequency Ω, the displacements in the transducer can be obtained. In order to solve this forced vibration problem, we have set up a FEM of surface acoustic wave generation in a periodic two-dimensional interdigital transducer on a piezoelectric substrate. The piezoelectric model follows the classical displacement-electric potential formulation in the frame of the quasi-static approximation of piezoelectricity [19]. The model is periodic along x_1 and infinite along x_2, and includes viscoelastic losses for both the substrate and the metal ridges. Compared to an actual experiment, it thus describes a transducer that is sufficiently long to be considered locally periodic—at least several tens of ridges are necessary—and the end effects are neglected. Specific FEM implementation details are given in Supplement 1.

Figure 3 shows the computed maximum absolute displacements as a function of driving frequency, for an applied potential difference of 1 V. More precisely, the FEM model provides the time-harmonic displacement field $u_i(\mathbf{r}; \Omega) \exp(i\Omega t)$, with $i = 1, 2, 3$. The maximum absolute displacement is defined as $\max_\mathbf{r}|u_i(\mathbf{r}; \Omega)|$. Within the frequency range from 0 to 6 GHz, there are four main resonances in the response, as listed in Table 1. All four resonances are subsonic, i.e., they appear below
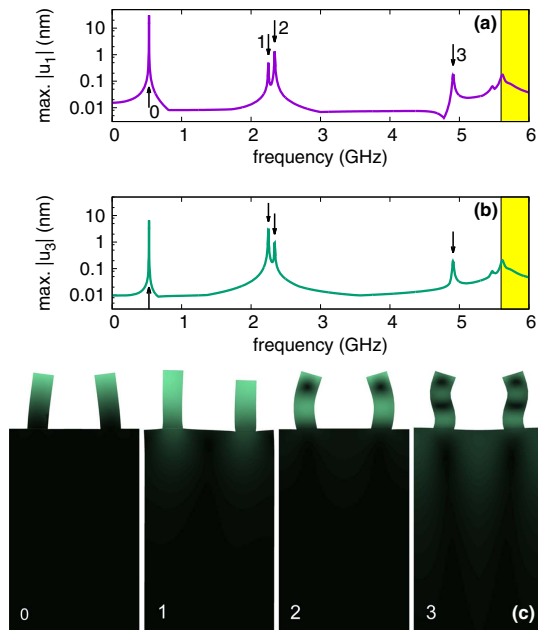

Fig. 3. Piezoelastic response of the structure. The maximum absolute displacements are shown as a function of frequency $\Omega/(2\pi)$ for an applied electric potential difference of 1 V, in (a) for longitudinal and in (b) for shear-vertical components. The yellow region marks the sound cone for the substrate. Acoustic modal shapes are illustrated in (c) for the four main resonances. The color scale is for the normalized total displacement. Note that vibration amplitudes have been adjusted for display purposes (see text).

Table 1. Resonant Frequencies and Maximum Absolute Displacements Are Given for the First Four Surface Acoustic Modes of Fig. 3, for a Potential Difference of 1 V

m	0	1	2	3
$\Omega_m/(2\pi)$ (GHz)	0.53	2.25	2.34	4.91
$\max|u_1|$ (nm)	30.6	0.5	1.3	0.2
$\max|u_3|$ (nm)	6.5	3.2	0.9	0.2

the sound cone, or in the nonradiative region of the substrate. Indeed, because of the periodicity of electrical excitation, the acoustic wavenumber $K = 2\pi/p$. In analogy with the light cone, the sound cone is defined by the condition $\Omega > v_s K$, with v_s the slowest bulk elastic wave. Given the period $p = 640$ nm and given that $v_s = 3590$ m/s for propagation along the Z crystallographic axis of lithium niobate [20], the sound cone starts at frequency $v_s/p = 5.6$ GHz. Below this value, all resonances are localized at the surface and do not radiate inside the bulk.

The vibration modes at the four resonances are depicted in Fig. 3. As the solution of the FEM problem provides the complex time-harmonic displacement fields, the actual motion for the mth resonant mode as a function of time is

$$\alpha_m \Re[u_i(\mathbf{r}; \Omega_m) \exp(i\Omega_m t)], \qquad (1)$$

where α_m is a scaling coefficient. Note that the vibration amplitudes in Fig. 3 have been adjusted for display purposes. The scaling coefficients in Eq. (1) are $\alpha_0 = 1$, $\alpha_1 = 10$, $\alpha_2 = 20$, and $\alpha_3 = 50$. They compensate for the different maximum absolute displacements listed in Table 1.

The vibration amplitudes are given for an infinite array of ridges and are effectively limited at resonance by viscoelastic losses in the ridges and the substrate. They must be expected to be reduced in an actual experiment with a finite-length structure. In practice, the vibration amplitude at a particular driving frequency can be controlled by the number of ridges in the structure and by the applied voltage. Previous SAW experiments indicate that vibration amplitudes of the order of several nanometers can be reached in arrays of pillars and ridges on a surface [21,22]. Given that the vibrations involved here are mostly flexural, rather large amplitudes of vibration at the top of the ridges—of the order of 10 nm or more—seem plausible. Note that displacements inside the substrate remain small compared to flexural displacements in the ridges.

4. EXTRAORDINARY AO MODULATION

We next consider the AO modulation problem: given an established vibration of the structure at a given driving frequency, what is the resulting modulation of the optical transmission? Let us first consider the limit of small deformations, which is the traditional approximation of acousto-optics. Within this limit, first-order perturbation theory gives AO coupling coefficients in the form of overlap integrals [12]. Since strains in the substrate remain small, we can safely ignore the photoelastic contribution here. See Supplement 1 for further justification of this approximation. Furthermore, the results to follow show that first-order perturbation theory is inadequate for the description of the moving interface effect in the considered structure. Instead, numerical analysis of the moving interface effect beyond the first-order approximation is rather easily performed under an adiabatic hypothesis.
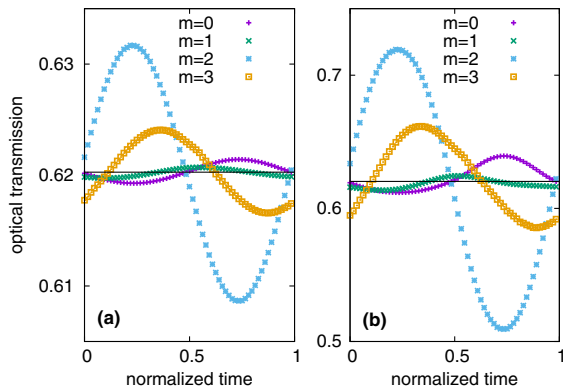
Fig. 4. AO modulation under small deformations. The modulation of the optical transmission caused by the various acoustic resonances is shown as a function of time in (a) and (b) for a maximum displacement limited to 100 pm and 1 nm, respectively. Normalized time is defined as $\Omega_m t/(2\pi)$, with Ω_m the resonant acoustic frequency. The optical wavelength is selected at the left inflection point in Fig. 2(a), or $\lambda = 1459.5$ nm, in order to obtain the maximum modulation.

Since the optical frequency is much larger than the acoustic frequency, one can consider that the acoustic motion appears as almost frozen to traveling optical waves, and that those have ample time to adapt to changes in the shape of the structure. Hence, the acoustic period can be decomposed in a sequence of successive snapshots for which the optical properties can be calculated. Such a procedure was previously implemented for one-dimensional structures [14], photonic crystal cavities [23], and optical waveguides [10].

For the results shown in Fig. 4, we selected the values α_m such that the maximum displacement of each acoustic mode is equal to either 100 pm or 1 nm. The AO modulation for a maximum displacement of 100 pm is mostly sinusoidal at the acoustic frequency for all modes. When the maximum displacement is increased to 1 nm, the modulation becomes nonlinear and higher harmonics of the acoustic frequencies are generated. Because of the renormalization of displacements in Fig. 4, the results may suggest that mode $m = 2$ is the most favorable for AO modulation. However, at fixed driving voltage, the flexural vibrations for mode $m = 0$ are 23.5 times larger than for mode $m = 2$, as Table 1 indicates. Hence, the fundamental flexural mode is actually causing the largest AO modulation among all four acoustic resonances.

We now address the effect of large acoustic deformations of the structure. Given the results for small deformations, we focus on the fundamental ($m = 0$) acoustic mode. Indeed, this mode exhibits mostly flexural oscillations of the ridges that cause a significant geometrical modification of the boundaries of the optical cavities. The maximum vibration amplitude is now taken as in Table 1 (i.e., $\alpha_0 = 1$), and the adiabatic AO modulation calculation is conducted again.

Figure 5(a) shows the variation of the optical transmission as a function of both time and optical wavelength. It is seen that, for a fixed wavelength, the transmission is strongly modulated as a function of time, and that this modulation is highly nonlinear. Indeed, the modulation remains rather limited for about one half of the acoustic period, with a small blue-shift, but is very strong during the remaining half period, with a large red-shift.
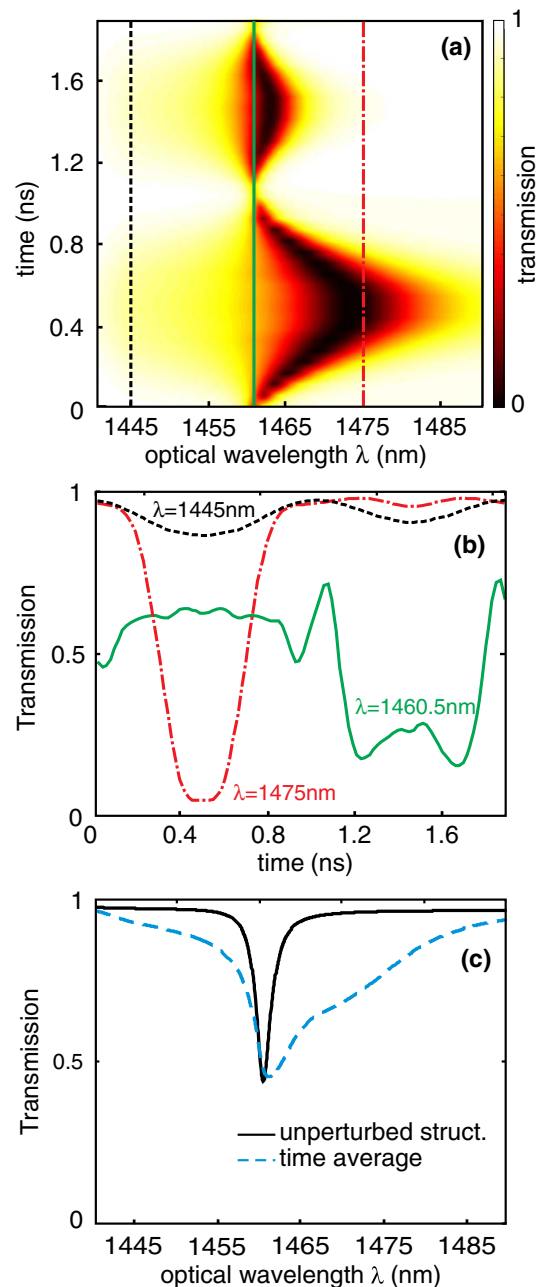

Fig. 5. AO modulation under full flexural motion. The modulation of the optical transmission spectrum is evaluated for the fundamental acoustic mode. The instantaneous optical spectrum is shown in (a) as a function of time (see Visualization 1). Three cross sections at constant optical wavelength are shown in (b) following the dotted lines in (a) (see Visualization 2). The time-averaged transmission spectrum is compared in (c) to transmission without deformation.

Visualization 1 shows the temporal evolution of the optical transmission spectrum. It is noteworthy that the optical reflection as a function of time and optical wavelength mostly complements the transmission (see Supplement 1). The AO structure could thus be operated alternatively in reflection mode.

The transmission is plotted in Fig. 5(b) for three values of the wavelength: $\lambda_1 = 1445$ nm, $\lambda_2 = 1460.5$ nm, and $\lambda_3 = 1475$ nm. Despite these wavelengths being rather close, the transmissions as a function of time are vastly dissimilar.

Visualization 2 shows the effect of the fundamental acoustic mode on the electric field intensity map and its propagating direction (Poynting vector) as a function of time at $\lambda_2 = 1460.5$ nm. The temporal modulations in Fig. 5(b) correspond to a possible experimental configuration where the optical transmission would be measured with a fast photodiode as a function of time, using a tunable single-frequency optical laser source.

Alternatively, one could attempt to capture the transmitted optical spectrum using a slow detector, for instance an optical spectrum analyzer, so that the time average of transmission could be obtained as a function of wavelength. Figure 5(c) displays such a spectrum. The numerical results then suggest that a clear distortion of the transmission spectrum could be observable directly on a spectrometer when the driving acoustic frequency is tuned to a vibration resonance of the structure.

5. DISCUSSION AND CONCLUSION

The results presented in Fig. 5 clearly suggest that the nonlinearity of the optical transmission as a function of time is a consequence of the rather narrow spectral transmission dip being displaced and broadened by the flexural motion of the vibrating ridges. This motion modulates the volume of the photonic cavities and hence the resonant optical frequency. Compared with recent attempts at designing periodic metal-dielectric structures showing enhanced AO modulation [24,25], a significant difference is that the ridges are here relatively free to vibrate with large amplitude, since they are attached to the substrate only at their base. Similar to the prongs of a tuning fork, each couple of ridges in a period of the array oscillates anti-symmetrically, creating a vibration node near the substrate surface that minimizes mechanical energy dissipation by radiation.

The mechanism behind AO modulation is also quite different from bulk AO devices relying on light diffraction by a propagating acoustic wave. An important difference is that the resonant modulation always increases with the amplitude of vibration of the ridges (see Supplement 1 for the extreme case that the displacement amplitude reaches the maximum value permitted before the oscillating ridges actually touch one another). In contrast, in a bulk AO device, the modulation varies periodically with the acoustic power and the interaction length.

As we already noted, the nonlinearity of the AO response of the structure far escapes the frame of first-order perturbation theory that is usually employed to describe AO interaction. Indeed, our numerical simulations imply that transmission modulation can approach 100% at GHz frequencies if flexural motion of the ridges reaches an amplitude of the order of 10 nm. This result suggests in turn to search for optomechanical structures where large mechanical motion could be induced all-optically, possibly resulting in strong optomechanical coupling. As a note, the structure discussed here is not an adequate candidate for strong optomechanical coupling as its optical quality factor is lower than required [7].

Finally, from an AO point of view, the doubly resonant structure achieves large transmission modulation although the thickness is only about one fifth of the optical wavelength. The interaction length is then several orders of magnitude smaller than in non-resonant AO devices. As a result, our study suggests ways to integrate efficient AO modulators in highly compact photonic devices.

See Supplement 1 for supporting content.

REFERENCES

1. L. Brillouin, "Diffusion de la lumière et des rayons X par un corps transparent homogène. Influence de l'agitation thermique," Ann. Phys. **9**, 88–122 (1922).
2. P. Debye and F. W. Sears, "On the scattering of light by supersonic waves," Proc. Natl. Acad. Sci. USA. **18**, 409–414 (1932).
3. R. Lucas and P. Biquard, "Propriétés optiques des milieux solides et liquides soumis aux vibrations élastiques ultra sonores," J. Phys. **71**, 464–477 (1932).
4. J. Xu and R. Stroud, *Acousto-Optic Devices: Principles, Design, and Applications* (Wiley, 1992).
5. T. J. Kippenberg and K. J. Vahala, "Cavity optomechanics: back-action at the mesoscale," Science **321**, 1172–1176 (2008).
6. A. H. Safavi-Naeini, T. M. Alegre, J. Chan, M. Eichenfield, M. Winger, Q. Lin, J. T. Hill, D. E. Chang, and O. Painter, "Electromagnetically induced transparency and slow light with optomechanics," Nature **472**, 69–73 (2011).
7. M. Aspelmeyer, T. J. Kippenberg, and F. Marquardt, "Cavity optomechanics," Rev. Mod. Phys. **86**, 1391–1452 (2014).
8. I. Favero and K. Karrai, "Optomechanics of deformable optical cavities," Nat. Photonics **3**, 201–205 (2009).
9. P. T. Rakich, C. Reinke, R. Camacho, P. Davids, and Z. Wang, "Giant enhancement of stimulated Brillouin scattering in the subwavelength limit," Phys. Rev. X **2**, 011008 (2012).
10. V. Laude and J.-C. Beugnot, "Lagrangian description of Brillouin scattering and electrostriction in nanoscale optical waveguides," New J. Phys. **17**, 125003 (2015).
11. J. E. Sipe and M. J. Steel, "A Hamiltonian treatment of stimulated Brillouin scattering in nanoscale integrated waveguides," New J. Phys. **18**, 045004 (2016).
12. Y. Pennec, V. Laude, N. Papanikolaou, B. Djafari-Rouhani, M. Oudich, S. El Jallal, J. C. Beugnot, J. M. Escalante, and A. Martínez, "Modeling light-sound interaction in nanoscale cavities and waveguides," Nanophotonics **3**, 413–440 (2014).
13. S. G. Johnson, M. Ibanescu, M. A. Skorobogatiy, O. Weisberg, J. D. Joannopoulos, and Y. Fink, "Perturbation theory for Maxwell's equations with shifting material boundaries," Phys. Rev. E **65**, 066611 (2002).
14. I. E. Psarobas, N. Papanikolaou, N. Stefanou, B. Djafari-Rouhani, B. Bonello, and V. Laude, "Enhanced acousto-optic interactions in a one-dimensional phoxonic cavity," Phys. Rev. B **82**, 174303 (2010).
15. D. C. Skigin and R. A. Depine, "Transmission resonances of metallic compound gratings with subwavelength slits," Phys. Rev. Lett. **95**, 217402 (2005).
16. A. Vial, "Implementation of the critical points model in the recursive convolution method for modelling dispersive media with the finite-difference time domain method," J. Opt. A **9**, 745–748 (2007).
17. I. M. Mandel, A. B. Golovin, and D. T. Crouse, "Fano phase resonances in multilayer metal-dielectric compound gratings," Phys. Rev. A **87**, 053847 (2013).
18. V. Laude, L. Robert, W. Daniau, A. Khelif, and S. Ballandras, "Surface acoustic wave trapping in a periodic array of mechanical resonators," Appl. Phys. Lett. **89**, 083515 (2006).
19. M. B. Dühring, V. Laude, and A. Khelif, "Energy storage and dispersion of surface acoustic waves trapped in a periodic array of mechanical resonators," J. Appl. Phys. **105**, 093504 (2009).
20. D. Royer and E. Dieulesaint, *Elastic Waves in Solids* (Wiley, 1999).
21. Y. Achaoui, A. Khelif, S. Benchabane, L. Robert, and V. Laude, "Experimental observation of locally-resonant and Bragg band gaps for surface guided waves in a phononic crystal of pillars," Phys. Rev. B **83**, 104201 (2011).

22. L. Socié, S. Benchabane, L. Robert, A. Khelif, and V. Laude, "Surface acoustic wave guiding in a diffractionless high aspect ratio transducer," Appl. Phys. Lett. **102**, 113508 (2013).

23. Q. Rolland, M. Oudich, S. El-Jallal, S. Dupont, Y. Pennec, J. Gazalet, J.-C. Kastelik, G. Leveque, and B. Djafari-Rouhani, "Acousto-optic couplings in two-dimensional phoxonic crystal cavities," Appl. Phys. Lett. **101**, 061109 (2012).

24. A. Mrabti, G. Lévêque, A. Akjouj, Y. Pennec, B. Djafari-Rouhani, R. Nicolas, T. Maurer, and P.-M. Adam, "Elastoplasmonic interaction in metal-insulator-metal localized surface plasmon systems," Phys. Rev. B **94**, 075405 (2016).

25. R. Ulbricht, H. Sakuma, Y. Imade, P. H. Otsuka, M. Tomoda, O. Matsuda, H. Kim, G.-W. Park, and O. B. Wright, "Elucidating gigahertz acoustic modulation of extraordinary optical transmission through a two-dimensional array of nano-holes," Appl. Phys. Lett. **110**, 091910 (2017).